

Greenhouse warming potential of a suite of gas species on early Mars evaluated using a radiative-convective climate model

JASON JORGE,¹ ROBIN WORDSWORTH,^{1,2} AND DANICA ADAMS¹

¹*Department of Earth and Planetary Sciences, Harvard University, Cambridge, MA, USA*

²*School of Engineering and Applied Sciences, Harvard University, Cambridge, MA, USA*

ABSTRACT

Abundant geomorphological and geochemical evidence of liquid water on the surface of early Mars during the late Noachian and early Hesperian periods needs to be reconciled with a fainter young Sun. While a dense CO₂ atmosphere and related warming mechanisms are potential solutions to the early Mars climate problem, further investigation is warranted. Here, we complete a comprehensive survey of the warming potential of all known greenhouse gases and perform detailed calculations for 15 different minor gas species under early Martian conditions. We find that of these 15 species, H₂O₂, HNO₃, NH₃, SO₂, and C₂H₄ cause significant greenhouse warming at concentrations of ~0.1 ppmv or greater. However, the most highly effective greenhouse gas species also tend to be more condensable, soluble and vulnerable to photolytic destruction. To provide a reference for future atmospheric evolution and photochemical studies, we have made our warming potential database freely available online.

1. PLAIN TEXT SUMMARY

Several billion years ago, geological evidence indicates that Mars was warmer and wetter, with flowing rivers and lakes on its surface. This is hard to explain because the Sun was fainter then, and Mars's orbit is more distant than Earth's. The atmosphere of early Mars was probably thicker, but additional greenhouse gases besides carbon dioxide are needed to provide enough warming. Here we perform a survey of the warming effect of all plausible greenhouse gases on early Mars. We isolate a few species that are particularly effective at warming the planet, calculate how much they raise temperatures at different concentrations, and discuss whether they could have built up to high concentrations in Mars's early atmosphere. Our work provides an important reference for future calculations that incorporate chemistry and other effects.

2. INTRODUCTION

Mars today is a cold and dry planet, with mean surface temperatures of around 210 K and a CO₂-dominated atmosphere less than 1% the volume of Earth's (Martínez et al. 2017). However, extensive geomorphological and geochemical evidence indicate that surface conditions were very different in its early history. Valley networks (Di Achille & Hynek 2010; Hynek et al. 2010), open-basin lakes (Fassett & Head 2008), and fluvial conglomerates (Williams et al. 2013) point to episodically warmer and wetter conditions, with particularly strong evidence for extensive surface alteration by liquid water

seen between ~3 and 3.8 Ga, based on crater counting chronology (Werner & Tanaka 2011).

Mars's distant orbit and the faintness of the young Sun mean that surface temperatures would have been well below zero in the absence of greenhouse warming from a thicker early atmosphere (Haberle et al. 2017; Wordsworth 2016). While a thicker CO₂ atmosphere can help solve the early martian climate problem, it does not appear sufficient alone (Forget et al. 2013; Wordsworth et al. 2013; Ramirez et al. 2014; Kerber et al. 2015; Kamada et al. 2021). Other dominant atmospheric constituents on early Mars are possible, such as H₂ or N₂, but are typically considered less likely.

Other solutions such as impact-induced steam atmospheres and SO₂-induced warming from volcanism have been proposed but suffer shortcomings that make them unlikely as primary explanations (Segura et al. 2002; Halevy et al. 2007; Segura et al. 2012; Halevy & Head 2014). Aerosols, including dust, volcanic sulfuric acid droplets and H₂O and CO₂ clouds have a variety of effects depending on their location and microphysical properties (Forget et al. 2013; Wordsworth et al. 2013; Urata & Toon 2013; Kerber et al. 2015; Kite et al. 2021; Steakley et al. 2023). Finally, reducing gases, particularly H₂, can cause strong warming in combination with CO₂ due to collision-induced absorption effects (Ramirez et al. 2014; Wordsworth et al. 2017; Turbet et al. 2019; Steakley et al. 2023). This appears to be a promising solution to the faint young Sun problem, but questions remain about how abundant such gases may

have been in the martian atmosphere through time, motivating further study.

There has not yet been a comprehensive survey of the warming potential of all known greenhouse gases on early Mars. Such an objective is important, because it can motivate future investigations that couple climate modeling to atmospheric chemical and study of sources and sinks. Here we survey the greenhouse warming potential of the entire HITRAN database (Gordon et al. 2022), and perform detailed calculations for 15 different minor gas species in the early Martian atmosphere. Computing the radiative potential of each of these gases across a wide range of mixing ratios under early Martian conditions, we provide a database of greenhouse warming for early Mars. In doing so, we expand the parameter space of possible warming mechanisms, and highlight gases for further investigation.

In Section 3, we discuss the one-dimensional radiative-convective model used to compute surface temperature and its validation, the selection of gas species, and our choices of uncertain parameters such as CO₂ line broadening coefficients. In Section 3, we discuss the results of our radiative calculations for all gases at 1 bar and the strongest absorbers at different CO₂ pressures. Finally, we discuss the possible sources and sinks of our strongest absorbers in Section 4.

3. METHODS

3.1. Model Description

We adapt the one-dimensional radiative-convective model PCM LBL (Wordsworth et al. 2021) to determine the increase in surface temperature due to the greenhouse effect of minor gas species on early Mars. This iterative line-by-line spectral code allows us to perform high accuracy globally averaged calculations across a wide range of atmospheric compositions.

PCM LBL calculates surface and atmospheric temperatures in equilibrium for a given solar flux, atmospheric composition and surface properties. Our model atmosphere is vertically divided into 50 layers from the surface to a minimum pressure of 1 Pa, and simulations were run for 300 time steps. Line data from the HITRAN2020 molecular spectroscopic database (Gordon et al. 2022) are used to compute absorption cross sections at wavenumber points on a temperature-log pressure grid of 12 interpolation points in 15 K intervals for each absorbing species. The vertical grid is set so that logarithms of pressure are evenly spaced, with their values determined by the initial conditions of surface temperature and surface pressure (Ding & Wordsworth 2019). As the model iterates toward the radiative-convective equilibrium state and the atmospheric tem-

perature profile shifts, new absorption cross sections are interpolated from this grid to calculate the adjusted monochromatic optical depth and radiative fluxes. To calculate absorption cross sections, line strengths are scaled from their reference values using the standard HITRAN formula (Gordon et al. 2022)

$$S_{ij}(T) = S_{ij}(T_0) \frac{Q(T_0)}{Q(T)} \frac{1 - e^{-h\nu_{ij}/k_B T}}{1 - e^{-h\nu_{ij}/k_B T_0}} \frac{e^{-h\nu_i/k_B T}}{e^{-h\nu_i/k_B T_0}} \quad (1)$$

where i and j represent the ground and excited states of the transition, respectively; S_{ij} is the line strength; Q is the total internal partition sum (TIPS); ν_{ij} is the line location; ν_i is the ground state frequency; T is the temperature; $T_0 = 296$ K is the reference temperature; h is the Planck constant; and k_B is the Boltzmann constant. Line broadening due to both collisional and Doppler effects are taken into account by representing lineshape as a Voigt profile via the Humlíček algorithm (Humlíček 1982; Wordsworth et al. 2017). Line position corrections due to pressure shifts are also included where HITRAN data is available (Gordon et al. 2022).

CO₂ is the bulk atmospheric constituent in all of our simulations. CO₂ pressures are varied between 0.5 and 2 bar based on estimates of the possible range of pressures during the late Noachian to early Hesperian periods (Hu et al. 2015; Jakosky 2019). CO₂ spectral lines are truncated at 500 cm⁻¹ to include sub-Lorentzian behavior of spectral lines far from the line center; for other gas species, spectral lines are truncated at 25 cm⁻¹ and pure Lorentzian behavior is assumed. We use 2000 wavenumber points for both shortwave and longwave calculations. Increases in spectral resolution did not strongly affect spectrally integrated flux and heating rates in the lower atmosphere or equilibrium surface temperature. To improve efficiency of the line-by-line calculation, we also removed weak lines from the HITRAN2020 data set, which we defined as lines with strengths below 1×10^{-30} cm⁻¹ / (molecule cm⁻²) at 1000 K. CO₂ collision-induced absorption (CIA) is calculated using the Gruszka-Borysov-Baranov (GBB) parameterization (Gruszka & Borysov 1998; Baranov et al. 2004; Wordsworth et al. 2010). Eight quadrature points total are used for shortwave and longwave radiative flux calculations, four upwelling and four downwelling. This eight-stream radiative calculation is computed at the pure-absorption limit.

The effects of Rayleigh scattering by CO₂ are included by increasing the reflectivity of the surface rather than the top of the atmosphere. This works because molecular absorption is only important in the thermal to near-IR for the atmospheres we are studying, while Rayleigh scattering occurs in visible and shorter wave-

lengths (Ding & Wordsworth 2019). The most recent version of PCM LBL can perform multiple scattering calculations (Ding & Wordsworth 2022), but the scattering effects of clouds and aerosols are neglected here for simplicity. The surface albedo before Rayleigh adjustment is applied is set to 0.2, a value appropriate for the present-day martian surface. Surface albedo is uncertain for early Mars. A basaltic unoxidized rock surface would have lower albedo, as would any regions of surface ocean unobscured by clouds. Conversely, clouds or oxidized dust in the atmosphere could raise albedo. However, global warming potential of a given greenhouse gas is not strongly dependent on our choice here.

To compute surface temperature, outgoing longwave radiation (OLR) is first calculated by integrating the monochromatic equation for upwelling radiative flux (Schaefer et al. 2016). The difference between OLR and absorbed shortwave radiation (ASR) is then used to iterate the model towards a steady-state surface temperature and atmospheric temperature profile, following Wordsworth et al. (2017). Here ASR is defined as

$$ASR = \frac{(1 - A_p)F_{sol}}{4}, \quad (2)$$

where A_p is the planetary albedo and F_{sol} is the solar flux. The solar flux is taken to be $F_{sol} = 0.75 \times 590 \text{ W m}^{-2}$ where 590 W m^{-2} is the Earth’s solar constant scaled by Mars’ average orbital distance and 0.75 is the approximate effect of the fainter early Sun during the late Noachian period.

H_2O abundance at each layer is calculated using the saturation vapor pressure curve and a tropospheric relative humidity value of $\alpha_{sat} = 0.8$ and a heat capacity of the atmosphere of $c_p = 800 \text{ J kg}^{-1} \text{ K}^{-1}$. When the profile becomes unstable to moist convection, it relaxes to a moist adiabatic profile. The atmospheric temperature profile is assumed to be a moist adiabat of H_2O or CO_2 until sub-saturation occurs, at which point the temperature profile relaxes to simple radiative equilibrium.

We tested for condensation of greenhouse gases by incorporating saturation vapor curves for minor species in PCM LBL. These curves were modeled using the Antoine equation using data from (Yaws 2015). We found that for the range of conditions we considered, condensation was important for two species: H_2O_2 and HNO_3 . Finally, for intercomparison of the output of PCM LBL with other 1D radiative-convective models such as Clima (Kasting 1988; Kopparapu et al. 2013) and the linearized flux evolution (LiFE) model developed by Robinson & Crisp (2018), see Ding & Wordsworth (2019).

3.2. Gas Selection

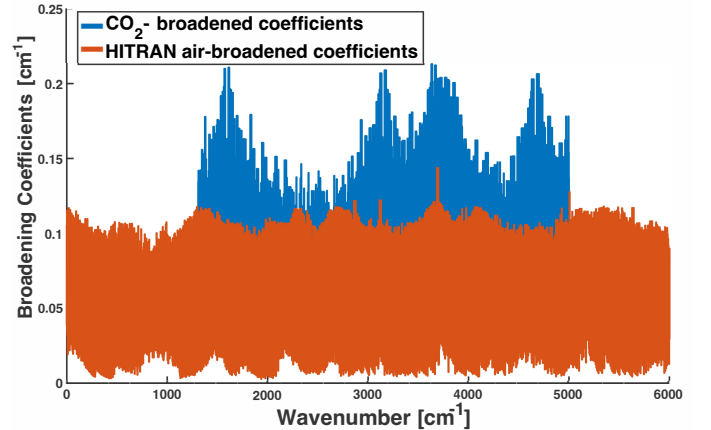


Figure 1. A comparison between CO_2 -broadening coefficients (Régalia et al. 2019) and air-broadening coefficients (Gordon et al. 2022) for H_2O . CO_2 -broadened coefficients appear to differ from air-broadened coefficients by a mean factor of ~ 1.6 , in agreement with a mean factor of 1.58 determined by Deichuli et al. (2022).

PCM LBL was used to calculate the greenhouse warming potential of O_3 , N_2O , CO , CH_4 , SO_2 , H_2S , NO_2 , NH_3 , HNO_3 , HBr , OCS , H_2CO , HCN , H_2O_2 , C_2H_6 , and C_2H_4 . These were selected from the list of all available gases with line-by-line data in the HITRAN2020 database (55 total). Many gases were excluded because they are unlikely to accumulate in any meaningful amount to act as an important greenhouse gas in the early Martian atmosphere. Radical species such as OH were excluded, for example, because they are highly reactive and very unlikely to accumulate to climatically important concentrations in the atmosphere. Other gases were excluded because of their low infrared absorptivity. For example, homonuclear diatomic molecules such as O_2 and N_2 were excluded because their electric dipole moment is zero and the molecules are IR-inactive, and collision-induced absorption is not important when the gas is a minor species.

3.3. CO_2 Line Broadening

Line-shape parameters such as air- and self-broadening coefficients (γ_L and γ_{self} respectively), the temperature exponent of air-broadening (n_{air}), and the air-pressure-induced line shift (δ_{air}) differ from one gas to another. While spectroscopic data for Earth-like (N_2 -dominated) atmospheres are abundant and well-constrained, estimates of broadening parameters for CO_2 -dominated atmospheres have only become available for a few species in recent years. The HITRAN2020 database contains pressure broadening parameters due to the ambient pressure of He , H_2 , and CO_2 gases (Tan

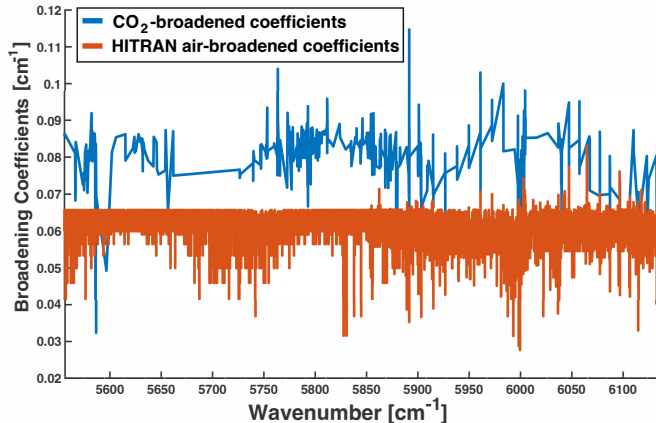


Figure 2. A comparison between CO_2 -broadening coefficients (Lyulin et al. 2014) and air-broadening coefficients (Gordon et al. 2022) for CH_4 . CO_2 -broadened coefficients appear to differ from air-broadened coefficients by a mean factor of ~ 1.33 .

et al. 2022), but these data are limited and not available for all of the gases in our sample.

To gauge the error in radiative calculations that may arise from using air-broadening parameters in a CO_2 -dominated atmosphere, we compare air-broadened coefficients (γ_{air}) for H_2O and CH_4 in the HITRAN2020 database to CO_2 -broadening parameters measured and calculated by Régalia et al. (2019) and Lyulin et al. (2014) respectively. As shown in Figure 1 above, H_2O broadening coefficients in CO_2 measured by Régalia et al. (2019) are ~ 1.6 times larger than H_2O broadening coefficients in air from the HITRAN2020 database, similar to the mean factor of 1.58 observed in Deichuli et al. (2022). Comparing the CO_2 -broadening coefficients for CH_4 produced by Lyulin et al. (2014) to air-broadened coefficients in the HITRAN2020 database, the mean factor appears to be ~ 1.33 as shown in Figure 2 above.

As a test, we ran PCM LBL using a 1-bar atmosphere composed of CO_2 , H_2O , and 1 ppmv of CH_4 with two sets of broadening coefficients: 1) air-broadened coefficients as in the HITRAN2020 database and 2) an estimation of CO_2 -broadened coefficients using the scaling factors of 1.58 and 1.33 for H_2O and CH_4 respectively. The difference in OLR and surface temperature was found to be small, the latter increasing by only ~ 0.8 K.

Based on the scaling factors for H_2O and CH_4 , we assume that doubling air-broadened parameters is a reasonable estimate of the upper bound of CO_2 -broadening coefficients. To test the impact of doubled broadening parameters on an effective greenhouse gas in our sample, we additionally ran PCM LBL with each set of broadening parameters for a 1 bar atmosphere of CO_2 , H_2O ,

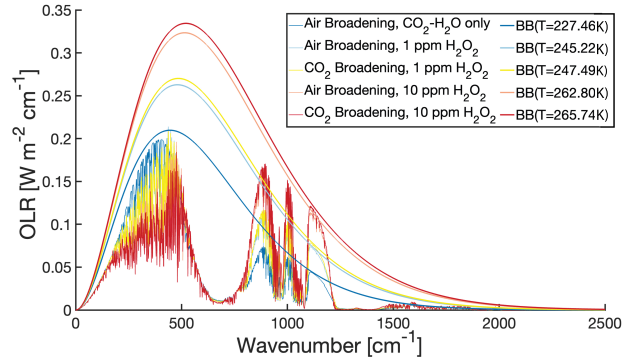


Figure 3. Comparison of OLR from a 1 bar atmosphere of CO_2 , H_2O , and 1 or 10 ppmv of H_2O_2 given air-broadening coefficients (HITRAN data) and a reasonable estimate of the upper bound of CO_2 -broadening coefficients. Differences in surface temperature between the two scenarios are on the order of ~ 1 -3K.

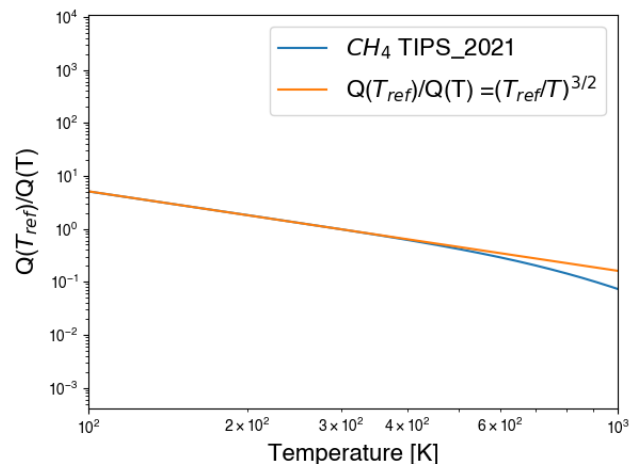


Figure 4. Comparison between TIPS and (3) for the first isotopologue of CH_4 between 100 K and 1000 K. (3) does not begin to significantly diverge from calculated TIPS ratios until ~ 400 K, well above the temperatures of the atmosphere of early Mars.

and 0, 1, or 10 ppmv of H_2O_2 . OLR as a function of wavenumber for each of these scenarios are shown in Figure 3. Overlaid on each OLR plot is a blackbody curve of the same color based on the surface temperature output by the model. Doubling the air-broadening coefficients of H_2O_2 to estimate the CO_2 -broadening coefficients increased the surface temperature ~ 2.2 K with 1 ppmv of H_2O_2 and ~ 3 K with 10 ppmv of H_2O_2 .

3.4. TIPS Ratio Approximation

The Total Internal Partition Sum (TIPS) is used to determine the population of molecules as a function of

Gas Species	GWP [ΔT (K)]
H ₂ O ₂	47.97
HNO ₃	42.51
SO ₂	17.67
C ₂ H ₄	13.00
NH ₃	11.07
O ₃	6.12
OCS	4.89
C ₂ H ₆	2.97
N ₂ O	1.56
NO ₂	1.28
H ₂ S	0.98
CH ₄	0.52
H ₂ CO	0.34
HCN	0.19
HBr	0.09
CO	0.04

Table 1. The difference in surface temperature between a CO₂-H₂O-only atmosphere and CO₂-H₂O atmosphere with 10 ppmv of each gas.

quantum state. These population factors determine the strength of vibrational-rotational transitions as seen in Equation 1 (Gamache et al. 2021). For CH₄, CO, H₂O, H₂S, HBr, N₂O, NH₃, NO₂, O₃, HCN, and H₂CO, we used a simple formula to approximate the TIPS ratio up to 1000 K, well above the reasonable set of temperatures we can expect in the early Martian atmosphere

$$Q(T_{ref})/Q(T) = (T_{ref}/T)^{1.5}. \quad (3)$$

Figure 4 shows that (3) closely matches actual CH₄ TIPS values between 100 K and 300 K. However, this approximation is bad at representing TIPS values of CO₂, SO₂, H₂O₂, C₂H₆, C₂H₄, HNO₃, and OCS between 100 K and 1000 K. Instead, TIPS values for these gases were approximated using an 8-degree least squares polynomial fit to actual TIPS data between 100 K and 1000 K, with r^2 values ranging between 0.968 and 0.983. Values used for these polynomials are given in Table 2.

4. RESULTS

4.1. Simulations of All Gases at 1 bar CO₂

PCM LBL produces surface temperatures of ~ 225 - 227 K given a 1 bar clear-sky atmosphere of CO₂ and H₂O under early Martian conditions, consistent with other modern radiative-convective models (Halevy & Head 2014; Ramirez et al. 2014; Wordsworth et al. 2010). After reaching radiative-convective equilibrium in a pure CO₂-H₂O atmosphere, we then add 0.001 to 500 ppmv

of each gas species¹ and again ran the model to equilibrium. Table 1 shows the difference in surface temperature between a CO₂-H₂O-only atmosphere and an atmosphere after adding 10 ppmv of each gas. We define this quantity as the global warming potential, or GWP.

We observe roughly three regimes of GWP in our sample: 1) At 10 ppmv, strong absorbers such as H₂O₂ and HNO₃ have GWPs above 40 K; 2) Moderate absorbers such as SO₂, C₂H₄, NH₃ have GWPs ranging from ~ 11 - 18 K; 3) and weak absorbers have GWPs ranging from ~ 0 - 6 K.

Figure 5 shows surface temperature [K] as a function of concentration [ppmv] for each gas species. Strong and moderate absorbers are shown on the left panel while the remainder are split between the middle and right panels. H₂O₂ and HNO₃ are the strongest absorbers across all tested concentrations and are able to warm the early Martian surface by multiple degrees, even at extremely low concentrations of 0.001 ppmv and 0.01 ppmv. At 10 ppmv and above, H₂O₂ and HNO₃ each push the surface temperature toward >273 K in our 1 bar atmosphere, demonstrating their uniquely high radiative potential. However, as the blue and green dashed lines indicate, these concentrations can only be achieved if the gases are supersaturated in the martian atmosphere. Condensation most severely limits H₂O₂ concentrations, causing greenhouse warming to be limited to a little over 230 K in that case.

Moderate absorbers such as SO₂, C₂H₄, and NH₃ begin to meaningfully warm the surface at concentrations ranging from 0.5 to 1 ppmv, with GWPs rising from ~ 4 - 7 K at 1 ppmv to ~ 20 - 28 K at 100 ppmv. The GWPs of the remaining gases at 10 ppmv range from 0.04 K to 6.1 K. While CO, HBr, HCN, and H₂CO have the smallest radiative effect across concentration parameter space, O₃, OCS, and C₂H₆ warm the surface by ~ 6.1 K, ~ 4.9 K, and ~ 3 K respectively. These gases could be important for warming early Mars, but higher concentrations are required to have a similar radiative impact to that of H₂O₂, HNO₃, and to a lesser extent SO₂, C₂H₄, and NH₃. While we do not focus on O₃, OCS, and C₂H₆ in the following discussion, future studies could also be conducted to evaluate their atmospheric sources and sinks on early Mars.

4.2. Simulations of Select Gases at 0.5 and 2 bars

From our radiative calculations of all gases at 1 bar, we narrow our focus to the five strongest absorbers in our

¹ Specific values used in the grid were: [0.001, 0.005, 0.01, 0.025, 0.05, 0.075, 0.1, 0.5, 1, 5, 10, 25, 50, 75, 100, 150, 200, 250, 350, 500] ppm.

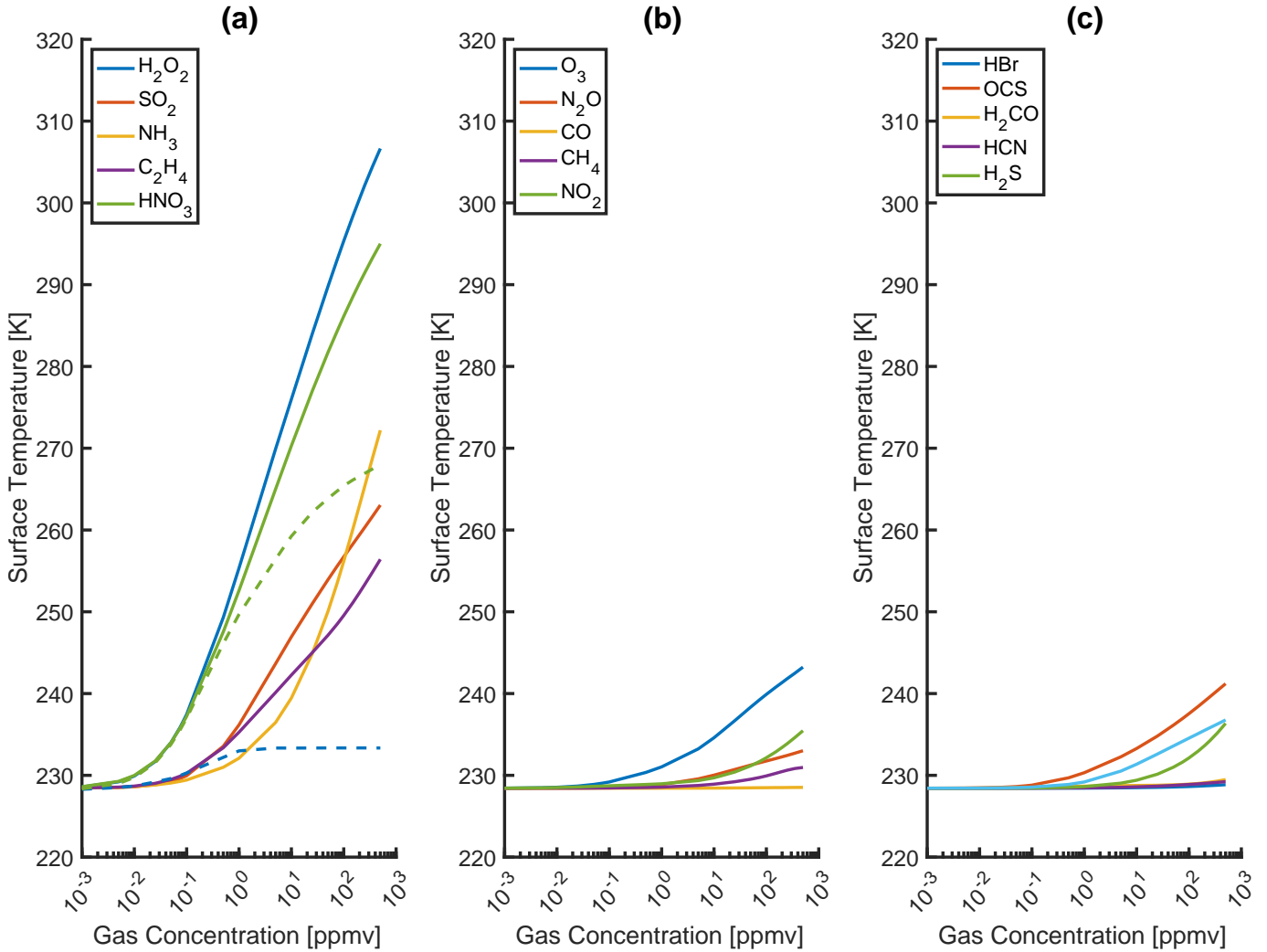


Figure 5. Surface temperature [K] vs. concentration [ppmv] for each gas in our sample, ranging from 0.001 ppmv to 500 ppmv. Strong and moderate absorbers are plotted on the left panel while weak absorbers are split between the middle and right panels for clarity. Dashed lines show warming when gas species concentration is limited by saturation. H_2O_2 and HNO_3 are the most effective greenhouse gases in our sample, and the most strongly affected by condensation.

sample: H_2O_2 , HNO_3 , SO_2 , C_2H_4 , and NH_3 . We simulate a clear-sky atmosphere of CO_2 and H_2O under early Martian conditions at 0.5 bars and 2 bars with the same concentrations as before, adding our strong and moderate absorbers. Given the total atmospheric pressure on early Mars is not well constrained, it is important to consider how the radiative effects of our strong and moderate absorbers change given different maximum surface pressures. Because the atmosphere collapses onto the surface completely at high enough CO_2 pressures (Kasting 1991; Forget et al. 2013; Soto et al. 2015) and there is not evidence for substantial carbon burial (Jakosky 2019; Hu et al. 2015; Wordsworth 2016), 2 bars is chosen to be an upper bound on total atmospheric pressure. Atmospheric collapse into ice caps can also occur at low total atmospheric pressures depending on the obliquity

of the planet, so 0.5 bars is chosen a lower bound on total atmospheric pressure.

The results of these radiative calculations are shown in Figure 6. At 0.5 bars, the differences between strong and moderate absorbers is more distinct. H_2O_2 and HNO_3 warm the surface ~ 10 K at 1 ppmv, ~ 20 K at 10 ppmv, and ~ 40 K at 100 ppmv. Each is capable of increasing surface temperature to >273 K alone, but only at the extreme end of our concentration parameter space (350-500 ppmv). In contrast, SO_2 , C_2H_4 , and NH_3 only warm the surface ~ 1 -3 K at 1 ppmv, ~ 5 -10 K at 10 ppmv, and ~ 10 -15 K at 100 ppmv. At 2 bars, there is less distinction between strong and moderate absorbers across the surface temperature-concentration parameter space. H_2O_2 and HNO_3 push the surface temperature to >273 K between 1 and 10 ppmv, while SO_2 and NH_3

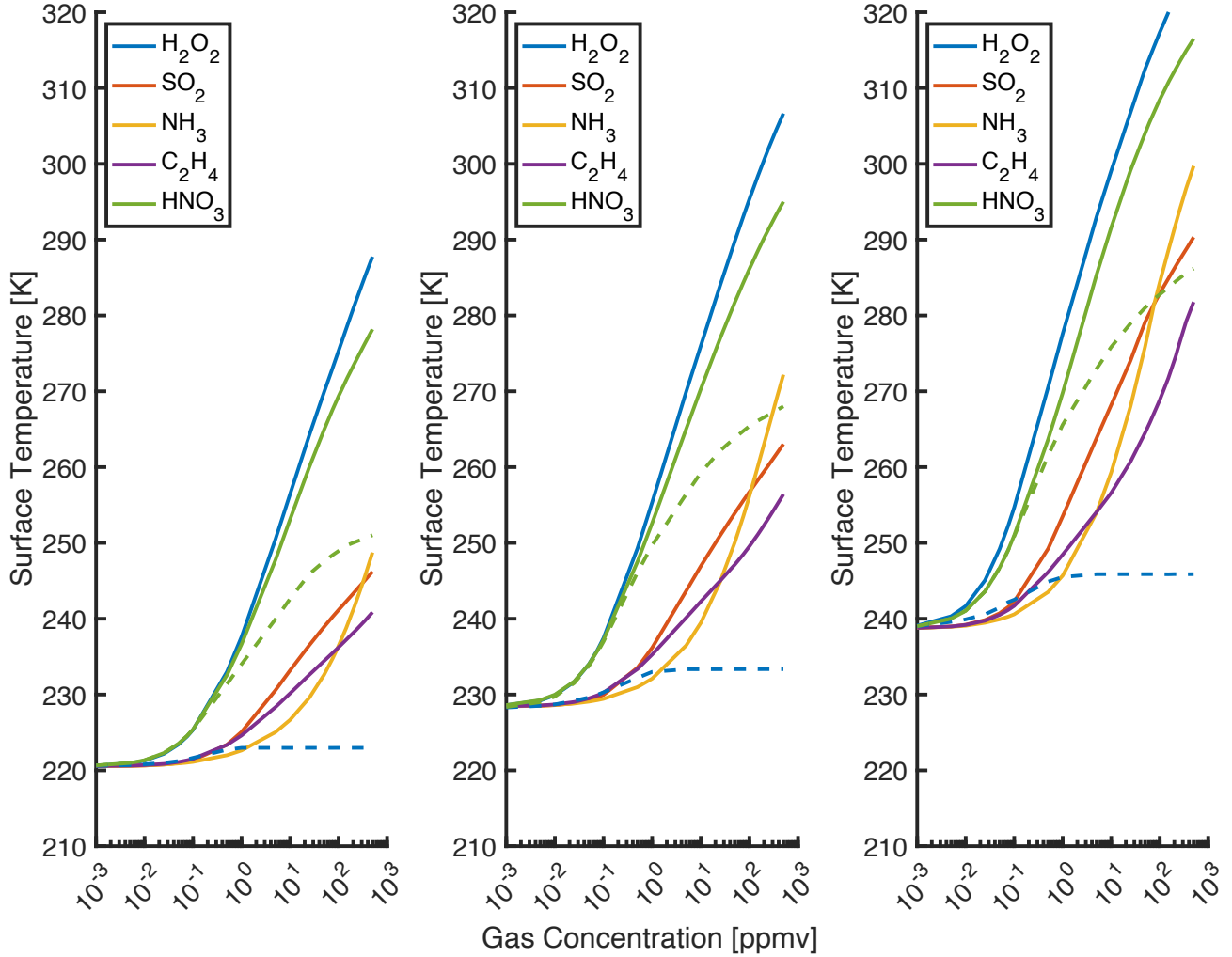


Figure 6. Surface temperature [K] vs. gas concentration [ppmv] of H_2O_2 , HNO_3 , SO_2 , C_2H_4 , and NH_3 at 0.5, 1, and 2 bars of total atmospheric pressure. As maximum surface pressure increases, so does the greenhouse effect induced by each gas.

do so close to 100 ppmv, and C_2H_4 does so at around 500 ppmv.

Figure 7 shows the temperature as a function of altitude from the surface to the top-of-atmosphere at 1 Pa for a 1 bar CO_2 - H_2O atmosphere with the addition of 10 ppmv of H_2O_2 , HNO_3 , SO_2 , C_2H_4 , and NH_3 . Each temperature-pressure profile shows temperature following a moist adiabat in the lower troposphere from the surface until about 0.5 bars, followed by CO_2 condensation in the middle atmosphere between ~ 0.01 and 0.1 bars where each profile converges. Above 0.01 bars, the profiles diverge as the upper atmosphere reaches radiative equilibrium. In this case, H_2O_2 and HNO_3 warm the surface 15-30 K more than SO_2 , C_2H_4 , and NH_3 .

H_2O_2 , HNO_3 , SO_2 , C_2H_4 , and NH_3 are effective greenhouse gases under early Martian conditions because they absorb in atmospheric window regions around 400 cm^{-1} and 1000 cm^{-1} . CO_2 is opaque due

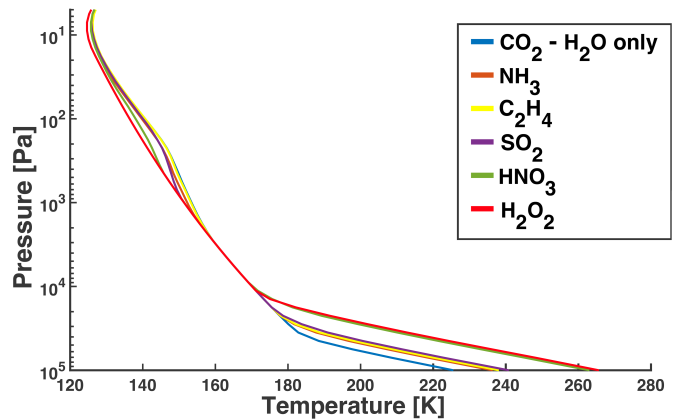


Figure 7. Temperature-pressure profiles of 1 bar CO_2 - H_2O atmospheres with the addition of 10 ppmv of H_2O_2 (red), HNO_3 (green), SO_2 (purple), C_2H_4 (yellow), and NH_3 (orange). A pure CO_2 - H_2O profile is also shown as a comparison (blue).

to the ν_2 667 cm^{-1} (15 μm) band (e.g., Goody & Yung 1995; Wordsworth et al. 2024) and CIA due to induced dipole effects around 1-250 cm^{-1} (Gruszka & Borysow 1998) and dimer effects from 1200-1500 cm^{-1} (Baranov et al. 2004). While CO_2 CIA absorption effects are taken into account, CO_2 CIA absorption bands are not included in absorption cross-section files. Water vapor is a strong absorber at low wavenumbers and at its ν_2 band at 1600 cm^{-1} .

Shown in Figure 8, H_2O_2 absorbs radiation at wavenumbers between 200 and 500 cm^{-1} , near the peak of the blackbody spectrum for a temperature of 265 K. H_2O_2 also has a strong absorption band centered around 1250 cm^{-1} . Absorption in these atmospheric window regions by H_2O_2 where there is not significant interference by CO_2 and H_2O absorption bands pushes the surface temperature toward 273 K, making it an effective greenhouse gas under early Martian conditions.

HNO_3 is a very effective greenhouse gas. Shown in Figure 9, HNO_3 has a strong absorption band centered just before 500 cm^{-1} near the peak of the blackbody spectrum at ~ 260 K. This absorption band only partially intersects H_2O absorption and avoids intersecting with the ν_2 667 cm^{-1} CO_2 absorption band. HNO_3 has another set of absorption bands centered around 800-1000 cm^{-1} , a region where there is neither strong CO_2 nor H_2O absorption. This absorption band plays a significant role in making HNO_3 an effective minor greenhouse gas under early Martian conditions.

SO_2 is a moderately effective greenhouse gas. Shown in Figure 10, SO_2 has an absorption band centered around 500 cm^{-1} , just to the right of the peak of the blackbody spectrum at 240 K. However, this absorption band intersects with the ν_2 667 cm^{-1} CO_2 absorption band. Because the atmosphere is already opaque at these wavelengths due to CO_2 absorption, SO_2 absorption has less of an effect on the surface temperature. While an SO_2 absorption band centered around 1100 cm^{-1} absorbs in an atmospheric window region and reduces OLR, absorption bands in the 1200-1500 cm^{-1} region partially intersect with CO_2 CIA absorption bands. This reduces SO_2 's effectiveness as a minor greenhouse gas compared to HNO_3 .

C_2H_4 is a moderately effective greenhouse gas. Shown in Figure 11, C_2H_4 has two main absorption bands centered around 1000 cm^{-1} and 1400 cm^{-1} . The 1000 cm^{-1} band absorbs in an atmospheric window region and is only intersected by weak pair of CO_2 absorption bands centered about 1000 cm^{-1} , avoiding intersecting with the ν_2 667 cm^{-1} CO_2 absorption band and CO_2 CIA absorption bands from 1200-1500 cm^{-1} . However, the C_2H_4 band centered around 1150 cm^{-1} intersects

with absorption by H_2O and is too far from the peak of the blackbody spectrum at 240 K to have an appreciable effect on surface temperature.

Finally, NH_3 is a moderately effective greenhouse gas. Shown in Figure 12, NH_3 has absorption bands centered around 100 cm^{-1} , 1000 cm^{-1} , and 1600 cm^{-1} . The absorption bands around 100 cm^{-1} and 1600 cm^{-1} are intersected by H_2O absorption and do not contribute to reductions in OLR, and the latter is far from the peak of the blackbody spectrum at ~ 240 K. While the NH_3 absorption band centered around 1000 cm^{-1} is only intersected by weak CO_2 absorption bands, it is very broad and less effective at absorption. Therefore, the reductions in OLR that arise from the portion of the NH_3 absorption band around 1000 cm^{-1} that is not intersected by CO_2 or H_2O absorption are only modest.

5. DISCUSSION

Our comprehensive survey deliberately focuses on the warming potential of all known greenhouse gases on early Mars to provide a database of greenhouse warming. While our detailed calculations show that numerous gases, including H_2O_2 , HNO_3 , NH_3 , SO_2 , and C_2H_4 , could act to warm the early Martian surface, it is important to couple climate modeling to atmospheric chemistry modeling and study sources and sinks to evaluate how much each greenhouse gas might accumulate in Mars' early atmosphere. Although this work is outside the scope of this paper, we qualitatively consider some of the wider context here.

When supersaturated concentrations are permitted, we find that H_2O_2 is the most effective minor greenhouse gas of those modeled, supporting the climate results of Ito et al. (2020). While H_2O_2 is the product of reactions between HOx species in a wet and oxidized atmosphere that may have existed at least episodically on early Mars (Hurowitz et al. 2017; Wordsworth et al. 2021), H_2O_2 condenses at low concentrations, is destroyed easily by photodissociation and rainout, as it is extremely soluble (Zahnle et al. 2008). Dry deposition is another potentially important removal mechanism of H_2O_2 , where the turbulence, solubility and reactivity of H_2O_2 , and the compositions and oxidation states of the surface affect the amount taken up at the surface.

HNO_3 is the second most effective minor greenhouse gas of those modeled. While the Mars Science Laboratory aboard Curiosity recently discovered nitrates in Gale Crater (e.g., Stern et al. 2015), HNO_3 has not been extensively studied as a potential greenhouse gas on early Mars. Adams et al. (2021) suggest possible mechanisms of nitrate deposition on early Mars due to both the formation of HNO_x from lightning-induced

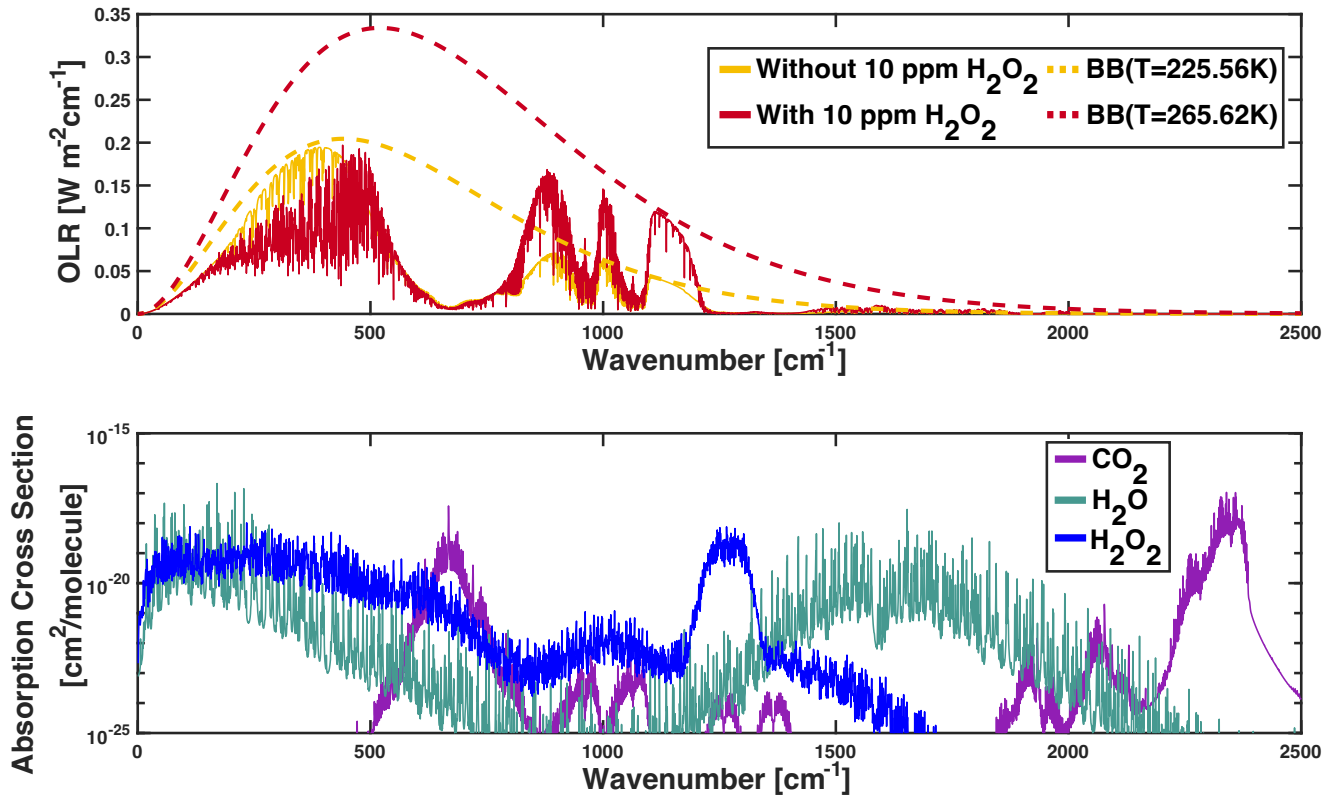


Figure 8. Upper panel: Outgoing planetary radiation as a function of wavenumber for a 1 bar atmosphere of CO_2 and H_2O with (red) and without (yellow) 10 ppmv of H_2O_2 . The dashed colored curves show blackbody radiation, of which the temperatures are indicated by $\text{BB}(T)$. Lower panel: Absorption cross sections of CO_2 (purple), H_2O (teal), and H_2O_2 (blue) at 1 bar, as functions of wavenumber.

NO , and splitting of N_2 by solar energetic particles created by coronal mass ejection events on the presumably more active young Sun. [Wong et al. \(2017\)](#) similarly propose that the CO_2 - N_2 dominated atmosphere of the Hadean Earth would, when heated by lightning, produce NO . NO would then react with water vapor to produce acids such as HNO , HNO_2 , and HNO_3 ([Wong et al. 2017](#)). [Adams et al. \(2021\)](#) studies the photochemical production and precipitation of HNO_x in an early Martian environment through a photochemistry and transport model, finding that HNO_3 is formed predominantly through the reaction of NO and HO_2 as in the mechanism proposed by [Wong et al. \(2017\)](#). The model used in [Adams et al. \(2021\)](#) also produces NO fluxes on early Mars similar to those calculated by [Wong et al. \(2017\)](#) for early Earth, suggesting the production of HNO_3 could occur on early Mars. However, as for H_2O_2 , the greatest challenge for HNO_3 is that it is relatively easy to condense and extremely soluble in water, making it extremely hard to build up in an atmosphere with an active hydrological cycle.

We find that SO_2 is one of the most effective minor greenhouse gases of those modeled. An SO_2 greenhouse on early Mars produced by extensive volcanism has been studied previously as a solution to the early Mars climate problem (e.g., [Halevy & Head 2014](#)), but SO_2 forms H_2SO_4 and elemental-sulfur aerosols in weeks to months following volcanic eruptions, causing cooling. The anti-greenhouse effect of these aerosols likely outweighs the greenhouse effect from sulfur gas in the long term ([Tian et al. 2010](#); [Kerber et al. 2015](#)). SO_2 is also rather soluble in water and easily removed from the atmosphere by rainout ([Johnson et al. 2009](#)).

Our radiative calculations also find that NH_3 acts as a potent greenhouse gas. Reducing gases such as CH_4 and NH_3 have been proposed as a solution to the early Mars climate problem, with [Sagan \(1977\)](#) suggesting that a hydrogen-dominated atmosphere or copious amounts of NH_3 could account for evidence of fluvial activity on the surface. Furthermore, [Kasting et al. \(1992\)](#) finds that 500 ppmv of NH_3 in a 4-5 bar CO_2 atmosphere could raise the surface temperature above 273 K. However, NH_3 is readily photolyzed by UV radiation on short time

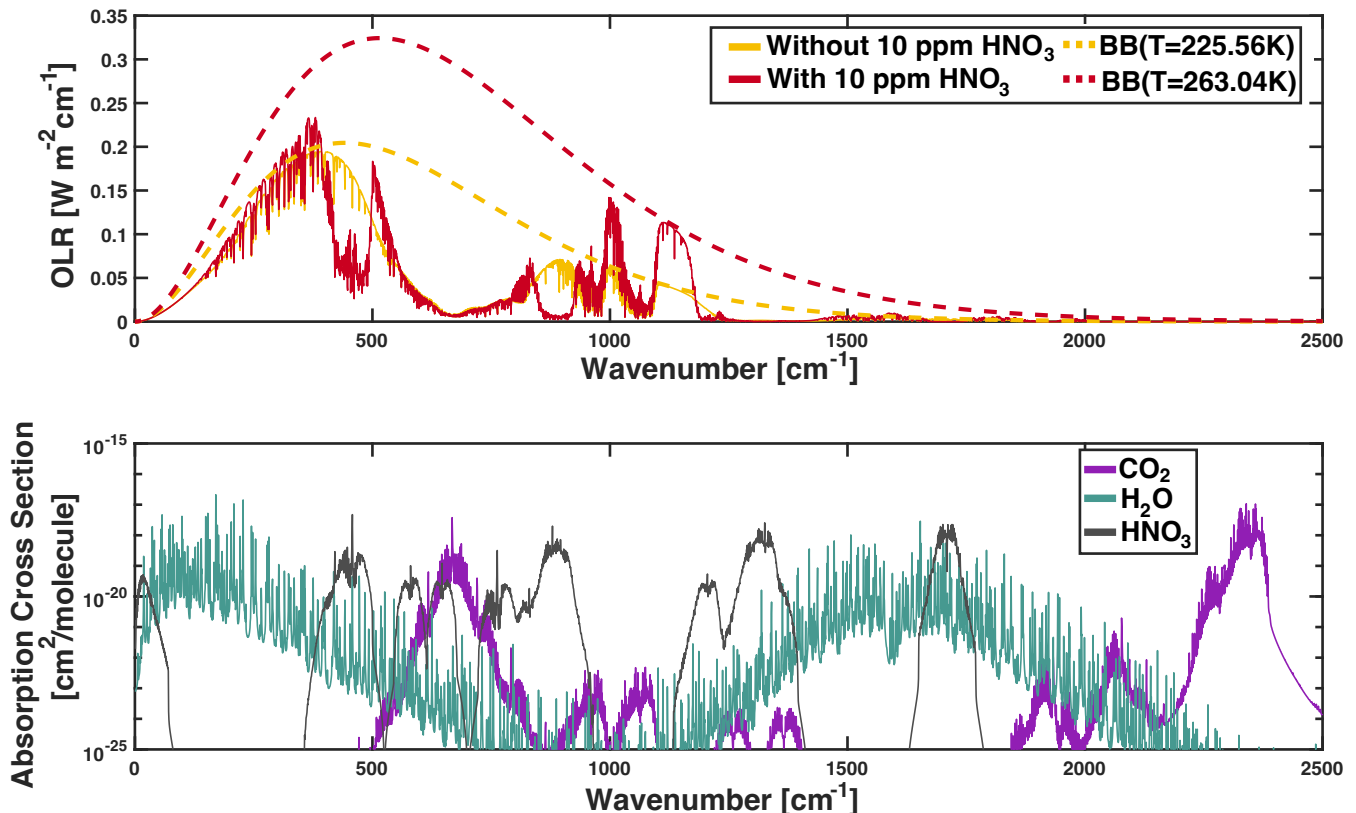


Figure 9. Upper panel: Outgoing planetary radiation as a function of wavenumber for a 1 bar atmosphere of CO₂ and H₂O with (red) and without (yellow) 10 ppm of HNO₃. The dashed colored curves show blackbody radiation, of which the temperatures are indicated by BB(T). Lower panel: Absorption cross sections of CO₂ (purple), H₂O (teal), and HNO₃ (grey) at 1 bar, as functions of wavenumber.

scales and there are not any significant plausible Martian sources. Appreciable concentrations of NH₃ could exist if there were a large surface or subsurface source and it was shielded from photolysis by an high-altitude organic haze (Sagan & Chyba 1997; Wolf & Toon 2010).

Finally, our radiative calculations show that C₂H₄ is a moderately effective greenhouse gas under early Martian conditions. While C₂H₄ photochemistry on early Mars has been considered as an eventual product of CH₄ photolysis and the reaction of methyl radicals, it has not been widely studied as a potential greenhouse gas. Haqq-Misra et al. (2008) investigate the radiative effects of a hazy methane greenhouse on the Archean Earth and argue that significant concentrations of CH₄ and solar UV radiation lead to the formation of higher-chain hydrocarbons such as C₂H₆ and C₂H₄, possible explanations for the Faint Young Sun paradox. Photolysis or oxidation of CH₄ leads to the formation of methyl radicals that can react to eventually form C₂H₄; significant concentrations of these gases are often accompanied by organic haze formation whose thickness determines

its net radiative effect (Haqq-Misra et al. 2008). Trainer et al. (2006) consider a similar organic haze on Titan and early Earth, arguing that the irradiation of a CH₄-N₂ atmosphere leads to the formation of aerosol particles that aggregate into fractal agglomerates and produce a thick haze layer. However, Trainer et al. (2006) note that haze photochemistry in a bulk CO₂ atmosphere likely differs from that observed on Titan. More photochemical modeling, ideally with additional laboratory data focused on haze formation in CH₄-CO₂ atmospheres, is needed to determine how much C₂H₄ could have warmed the early climate.

6. CONCLUSION

We have performed the first general survey of the warming potential of greenhouse gases on early Mars. Our analysis has revealed several important phenomena. First, the most radiatively active gas species also tend to be those that are highly soluble and/or vulnerable to photolytic destruction. This can be explained qualitatively by the fact that molecules with a large number of vibrational and rotational states are often polar, which

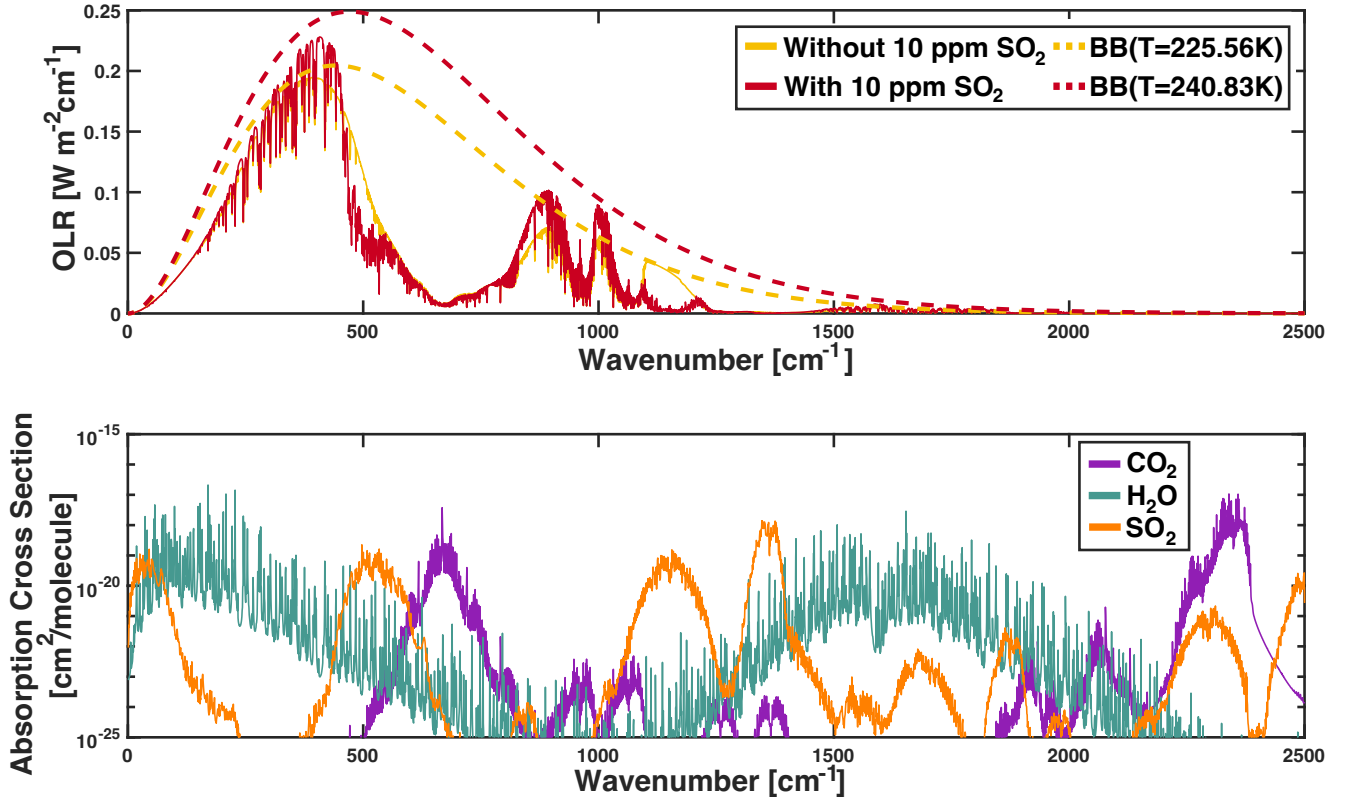


Figure 10. Upper panel: Outgoing planetary radiation as a function of wavenumber for a 1 bar atmosphere of CO_2 and H_2O with (red) and without (yellow) 10 ppmv of SO_2 . The dashed colored curves show blackbody radiation, of which the temperatures are indicated by $\text{BB}(T)$. Lower panel: Absorption cross sections of CO_2 (purple), H_2O (teal), and SO_2 (orange) at 1 bar, as functions of wavenumber.

allows them to dissolve easily in liquid water, and also makes them easy to break apart with moderately high energy photons.

We find that both reducing (C_2H_4 , NH_3) and oxidizing (H_2O_2 , HNO_3 , SO_2) minor species have the ability to cause greenhouse warming when present in high enough concentrations. This is interesting in the context of the martian geologic record, which strongly suggests that Mars has passed through both reducing and oxidizing atmospheric states in the past, with a slow trend to more oxidizing conditions over geologic time driven by loss of H to space (Hurowitz et al. 2017; Wordsworth et al. 2021; Liu et al. 2021; Jakosky et al. 2018).

This study has focused on background atmospheres dominated by CO_2 , and addition of N_2 to the calculations (e.g., Hu & Thomas 2022) could be expected to have some effect on the results. Additional climatic limitations of this study are that we have neglected 3D atmospheric dynamics and cloud radiative effects. Although such an assumption is standard in one-dimensional radiative-convective modeling, clouds can affect the radiative forcing of greenhouse gases via

both scattering and absorption, with the severity of the modification dependent on microphysics and global distribution. This could be addressed in future with 3D GCM simulations. However, the most important next step will be to use photochemical models with realistic representations of sources and sinks, in order to evaluate the plausibility of high enough concentrations to cause greenhouse warming for any of the species modeled here.

7. ACKNOWLEDGEMENTS

Support for this work was provided by NSF CAREER award AST-1847120 and NASA VPL award UWSC10439. The authors would like to thank Jake Seeley for helpful comments on line-by-line radiative calculations and Iouli Gordon for insight into the HITRAN spectroscopic database and TIPS calculations.

8. DATA AVAILABILITY STATEMENT

Surface temperature data tables, as well as the source code for the PCM LBL model used to produce all figures in the study, are available open-source

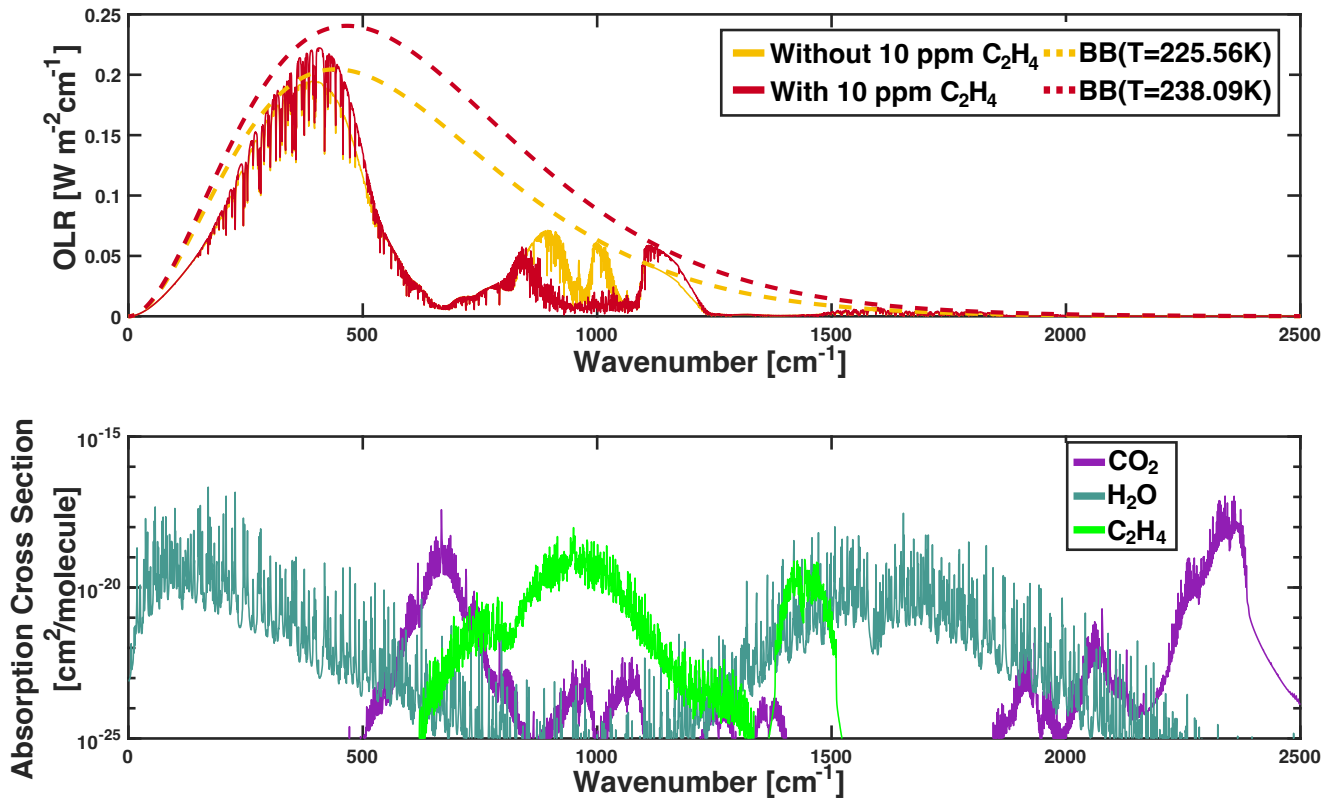


Figure 11. Upper panel: Outgoing planetary radiation as a function of wavenumber for a 1 bar atmosphere of CO₂ and H₂O with (red) and without (yellow) 10 ppmv of C₂H₄. The dashed colored curves show blackbody radiation cu, of which the temperatures are indicated by BB(T). Lower panel: Absorption cross sections of CO₂ (purple), H₂O (teal), and C₂H₄ (green) at 1 bar, as functions of wavenumber.

at <https://zenodo.org/records/13774100> (Jorge et al. 2024).

9. APPENDIX

REFERENCES

- Adams, D., Luo, Y., Wong, M. L., et al. 2021, *Astrobiology*, 21, 968
- Baranov, Y. I., Lafferty, W. J., & Fraser, G. T. 2004, Infrared spectrum of the continuum and dimer absorption in the vicinity of the O₂ vibrational fundamental in O₂/CO₂ mixtures
- Deichuli, V. M., Petrova, T. M., Solodov, A. M., Solodov, A. A., & Fedorova, A. A. 2022, *J. Quant. Spectrosc. Radiat. Transf.*, 293, 108386
- Di Achille, G., & Hynek, B. M. 2010, *Nat. Geosci.*, 3, 459
- Ding, F., & Wordsworth, R. D. 2019, A New Line-by-line General Circulation Model for Simulations of Diverse Planetary Atmospheres: Initial Validation and Application to the Exoplanet GJ 1132b
- . 2022, *The Astrophysical Journal Letters*, 925, L8
- Fassett, C. I., & Head, J. W. 2008, *Icarus*, 198, 37
- Forget, F., Wordsworth, R., Millour, E., et al. 2013, *Icarus*, 222, 81
- Gamache, R. R., Vispoel, B., Rey, M., et al. 2021, Total internal partition sums for the HITRAN2020 database
- Goody, R. M., & Yung, Y. L. 1995, *Atmospheric Radiation: Theoretical Basis* (Oxford University Press)
- Gordon, I. E., Rothman, L. S., Hargreaves, R. J., et al. 2022, *J. Quant. Spectrosc. Radiat. Transf.*, 277, 107949
- Gruszka, M., & Borysow, A. 1998, Computer simulation of the far infrared collision induced absorption spectra of gaseous CO₂
- Haberle, R. M., Todd Clancy, R., Forget, F., Smith, M. D., & Zurek, R. W. 2017, *The Atmosphere and Climate of Mars* (Cambridge University Press)
- Halevy, I., & Head, III, J. W. 2014, *Nat. Geosci.*, 7, 865

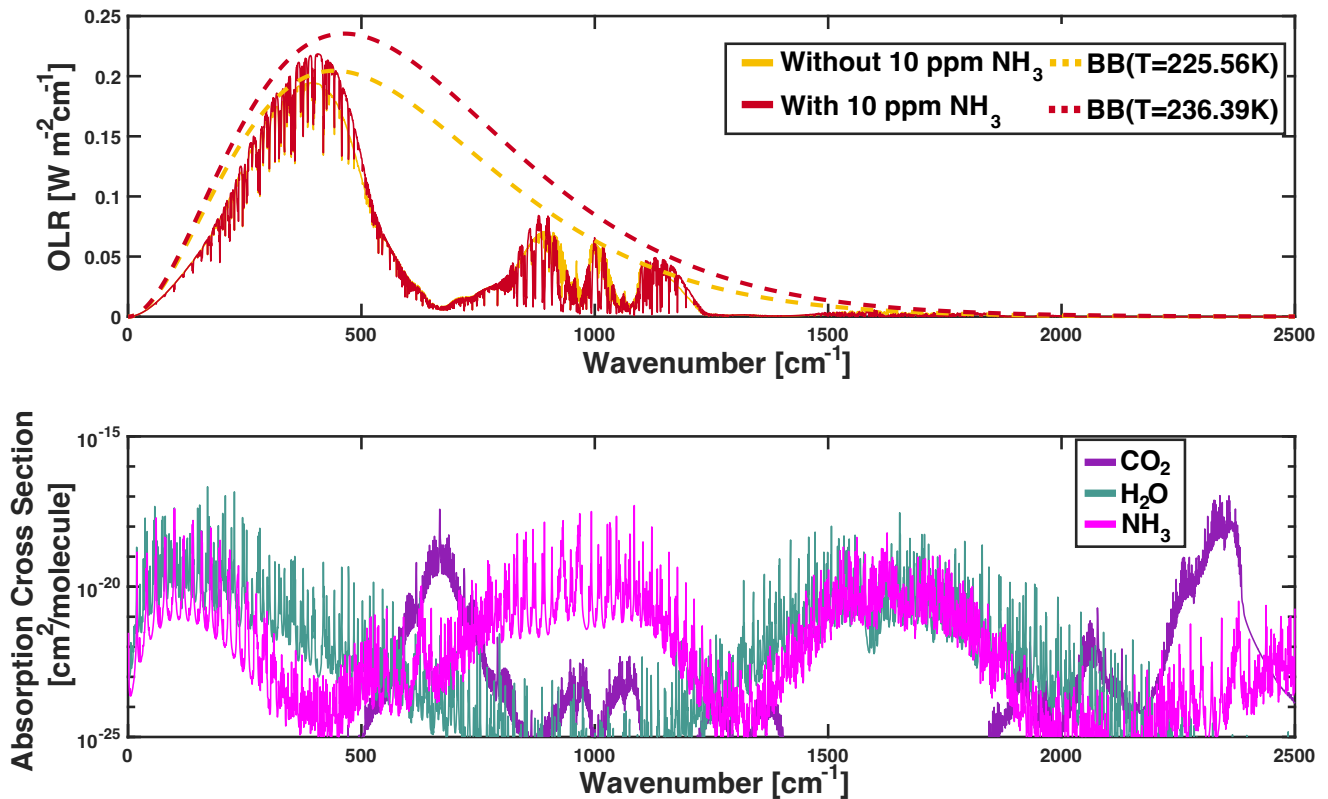


Figure 12. Upper panel: Outgoing planetary radiation as a function of wavenumber for a 1 bar atmosphere of CO₂ and H₂O with (red) and without (yellow) 10 ppmv of NH₃. The dashed colored curves show blackbody radiation, of which the temperatures are indicated by BB(T). Lower panel: Absorption cross sections of CO₂ (purple), H₂O (teal), and NH₃ (pink) at 1 bar, as functions of wavenumber.

Halevy, I., Zuber, M. T., & Schrag, D. P. 2007, *Science*, 318, 1903

Haqq-Misra, J. D., Domagal-Goldman, S. D., Kasting, P. J., & Kasting, J. F. 2008, *Astrobiology*, 8, 1127

Hu, R., Kass, D. M., Ehlmann, B. L., & Yung, Y. L. 2015, *Nat. Commun.*, 6, 1

Hu, R., & Thomas, T. B. 2022, *Nature Geoscience*, 15, 106

Humlíček, J. 1982, *J. Quant. Spectrosc. Radiat. Transf.*, 27, 437

Hurowitz, J. A., Grotzinger, J. P., Fischer, W. W., et al. 2017, *Science*, 356

Hynek, B. M., Beach, M., & Hoke, M. R. T. 2010, *J. Geophys. Res.*, 115

Ito, Y., Hashimoto, G. L., Takahashi, Y. O., Ishiwatari, M., & Kuramoto, K. 2020, *ApJ*, 893, 168

Jakosky, B. M. 2019, *Planet. Space Sci.*, 175, 52

Jakosky, B. M., Brain, D., Chaffin, M., et al. 2018, *Icarus*, 315, 146

Johnson, S. S., Pavlov, A. A., & Mischna, M. A. 2009, *J. Geophys. Res.*, 114

[Dataset] Jorge, J., Wordsworth, R., & Adams, D. 2024, <https://doi.org/10.5281/zenodo.13774100>

Kamada, A., Kuroda, T., Kasaba, Y., Terada, N., & Nakagawa, H. 2021, *Icarus*, 368, 114618

Kasting, J. F. 1988, *Icarus*, 74, 472

—. 1991, *Icarus*, 94, 1

Kasting, J. F., Brown, L. L., Acord, J. M., & Pollack, J. B. 1992, In *Lunar and Planetary Inst., Workshop on the Martian Surface and Atmosphere Through Time* p 84-85 (SEE N92-28988 19-91)

Kerber, L., Forget, F., & Wordsworth, R. 2015, *Icarus*, 261, 133

Kite, E. S., Steele, L. J., Mischna, M. A., & Richardson, M. I. 2021, *Proceedings of the National Academy of Sciences*, 118, e2101959118

Kopparapu, R. K., Ramirez, R., Kasting, J. F., et al. 2013, *ApJ*, 765, 131

Liu, J., Michalski, J. R., Tan, W., et al. 2021, *Nature Astronomy*, 5, 503

Table 2. Coefficients of the total internal partition sum polynomial $Q(T) = a_0 + a_1T + a_2T^2 + \dots + a_8T^8$ for different gases.

Gas Type	a_0	a_1	a_2	a_3	a_4	a_5	a_6	a_7	a_8
H ₂ O ₂	51.906	-0.736	0.0049	-1.867×10 ⁻⁵	4.37×10 ⁻⁸	-6.36×10 ⁻¹¹	5.617×10 ⁻¹⁴	-2.749×10 ⁻¹⁷	5.718×10 ⁻²¹
HNO ₃	51.578	-0.718	0.0047	-1.794×10 ⁻⁵	4.21×10 ⁻⁸	-6.156×10 ⁻¹¹	5.454×10 ⁻¹⁴	-2.678×10 ⁻¹⁷	5.585×10 ⁻²¹
C ₂ H ₆	55.45	-0.769	0.005	-1.918×10 ⁻⁵	4.474×10 ⁻⁸	-6.501×10 ⁻¹¹	5.727×10 ⁻¹⁴	-2.798×10 ⁻¹⁷	5.813×10 ⁻²¹
CO ₂	13.50	-0.156	0.000968	-3.613×10 ⁻⁶	8.37×10 ⁻⁹	-1.217×10 ⁻¹¹	1.065×10 ⁻¹⁴	-5.197×10 ⁻¹⁸	1.078×10 ⁻²¹
C ₂ H ₄	36	-0.499	0.0033	-1.271×10 ⁻⁵	2.982×10 ⁻⁸	-4.347×10 ⁻¹¹	3.838×10 ⁻¹⁴	-1.878×10 ⁻¹⁷	3.905×10 ⁻²¹
SO ₂	36.47	-0.502	0.0033	-1.262×10 ⁻⁵	2.954×10 ⁻⁸	-4.302×10 ⁻¹¹	3.799×10 ⁻¹⁴	-1.86×10 ⁻¹⁷	3.87×10 ⁻²¹
OCS	15.99	-0.181	0.0011	-4.099×10 ⁻⁶	9.507×10 ⁻⁹	-1.381×10 ⁻¹¹	1.218×10 ⁻¹⁴	-5.964×10 ⁻¹⁸	1.241×10 ⁻²¹

- Lyulin, O. M., Petrova, T. M., Solodov, A. M., Solodov, A. A., & Perevalov, V. I. 2014, *J. Quant. Spectrosc. Radiat. Transf.*, 147, 164
- Martínez, G. M., Newman, C. N., De Vicente-Retortillo, A., et al. 2017, *Space Sci. Rev.*, 212, 295
- Ramirez, R. M., Kopparapu, R., Zugger, M. E., et al. 2014, *Nat. Geosci.*, 7, 59
- Régalia, L., Cousin, E., Gamache, R. R., et al. 2019, Laboratory measurements and calculations of line shape parameters of the H₂O–CO₂ collision system
- Robinson, T. D., & Crisp, D. 2018, *J. Quant. Spectrosc. Radiat. Transf.*, 211, 78
- Sagan, C. 1977, *Nature*, 269, 224
- Sagan, C., & Chyba, C. 1997, *Science*, 276, 1217
- Schaefer, L., Wordsworth, R. D., Berta-Thompson, Z., & Sasselov, D. 2016, *Astrophys. J.*, 829, 63
- Segura, T. L., McKay, C. P., & Toon, O. B. 2012, *Icarus*, 220, 144
- Segura, T. L., Toon, O. B., Colaprete, A., & Zahnle, K. 2002, *Science*, 298, 1977
- Soto, A., Mischna, M., Schneider, T., Lee, C., & Richardson, M. 2015, *Icarus*, 250, 553
- Steakley, K. E., Kahre, M. A., Haberle, R. M., & Zahnle, K. J. 2023, *Icarus*, 394, 115401
- Stern, J. C., Sutter, B., Freissinet, C., et al. 2015, *Proc. Natl. Acad. Sci. U. S. A.*, 112, 4245
- Tan, Y., Skinner, F. M., Samuels, S., et al. 2022, *ApJS*, 262, 40
- Tian, F., Claire, M. W., Haqq-Misra, J. D., et al. 2010, *Earth Planet. Sci. Lett.*, 295, 412
- Trainer, M. G., Pavlov, A. A., Langley DeWitt, H., et al. 2006, Organic haze on Titan and the early Earth
- Turbet, M., Tran, H., Pirali, O., et al. 2019, *Icarus*, 321, 189
- Urata, R. A., & Toon, O. B. 2013, *Icarus*, 226, 229
- Werner, S. C., & Tanaka, K. L. 2011, *Icarus*, 215, 603
- Williams, R. M. E., Grotzinger, J. P., Dietrich, W. E., et al. 2013, *Science*, 340, 1068
- Wolf, E. T., & Toon, O. B. 2010, *Science*, 328, 1266
- Wong, M. L., Charnay, B. D., Gao, P., Yung, Y. L., & Russell, M. J. 2017, *Astrobiology*, 17, 975
- Wordsworth, R., Forget, F., & Eymet, V. 2010, *Icarus*, 210, 992
- Wordsworth, R., Forget, F., Millour, E., et al. 2013, *Icarus*, 222, 1
- Wordsworth, R., Kalugina, Y., Lokshantov, S., et al. 2017, *Geophys. Res. Lett.*, 44, 665
- Wordsworth, R., Knoll, A. H., Hurowitz, J., et al. 2021, *Nat. Geosci.*, 14, 127

Wordsworth, R., Seeley, J. T., & Shine, K. P. 2024, *The Planetary Science Journal*, 5, 67,

doi: [10.3847/PSJ/ad226d](https://doi.org/10.3847/PSJ/ad226d)

Wordsworth, R. D. 2016, *Annu. Rev. Earth Planet. Sci.*, 44, 381

Yaws, C. L. 2015, *The Yaws handbook of vapor pressure: Antoine coefficients* (Gulf Professional Publishing)

Zahnle, K., Haberle, R. M., Catling, D. C., & Kasting, J. F. 2008, *J. Geophys. Res.*, 113